poly-methyltrioxorhenium $\{(CH_3)_{0.92}ReO_3\}_\infty$: A conducting two-dimensional organometallic oxide

R. Miller, E.-W. Scheidt, G. Eickerling, C. Helbig, F. Mayr, R. Herrmann, and W. Scherer*
Chemische Physik und Materialwissenschaften, Universität Augsburg, 86159 Augsburg, Germany

H.-A. Krug von Nidda
Experimentalphysik V, Elektronische Korrelationen und Magnetismus, Universität Augsburg, 86159 Augsburg, Germany

V. Eyert and P. Schwab
Theoretische Physik II, Universität Augsburg, 86159 Augsburg, Germany
(Received 21 December 2005; published 13 April 2006)

Polymeric methyltrioxorhenium, $\{(CH_3)_{0.92}ReO_3\}_\infty$ (*poly*-MTO), is a prominent member of the organometallic hybrids which adopts the structural pattern and physical properties of classical perovskites in two dimensions (2D). We demonstrate how the electronic structure of *poly*-MTO can be tailored by an intercalation of organic donor molecules, such as tetrathiafulvalene (TTF) or bis-(ethylendithio)-tetrathiafulvalene (BEDT-TTF), and by the inorganic acceptor SbF_3. The integration of donor molecules leads to a more insulating behavior of *poly*-MTO, whereas the SbF_3 insertion does not cause any significant change in the resistivity. In particular, with increasing donor intercalation the metallic behavior of the parent compound, *poly*-MTO, becomes surprisingly suppressed leading to an insulator at TTF (BEDT-TTF) donor concentrations above 50% (25%). The resistivity data of pure *poly*-MTO exhibit a crossover from metallic ($d\rho/dT>0$) to insulating ($d\rho/dT>0$) behavior at a characteristic temperature around $T_{min}\simeq 38$ K. Above T_{min} the resistivity $\rho(T)$ is remarkably well described by a two-dimensional electron system. Below T_{min} an unusual resistivity behavior, similar to that found in doped cuprates, is observed: The resistivity initially increases approximately as $\rho\sim\ln(1/T)$ before it changes into a $\sqrt{T}$ dependence below 2 K. As an explanation we suggest a crossover from purely two-dimensional charge-carrier diffusion within the $\{ReO_2\}_\infty$ planes at high temperatures to three-dimensional diffusion at low temperatures in a disorder-enhanced electron-electron interaction scenario (Altshuler-Aronov correction). Furthermore, a linear positive magnetoresistance was found in the insulating regime, which is caused by spatial localization of itinerant electrons at some of the Re atoms, which formally adopt a $5d^1$ electronic configuration. X-ray diffraction, IR, and ESR studies, temperature dependent magnetization, and specific heat measurements in various magnetic fields suggest that the electronic structure of *poly*-MTO can safely be approximated by a purely 2D conductor which is labile towards spatial localization of electrons under the formation of Re(d^1) centers in the presence of a magnetic field.

DOI: 10.1103/PhysRevB.73.165113 PACS number(s): 71.20.Rv, 71.30.+h, 72.80.Le, 73.61.Ph

I. INTRODUCTION

The metal-oxide polymeric methyltrioxorhenium $\{(CH_3)_{0.92}ReO_3\}_\infty$ (*poly*-MTO) is a remarkable representative of an inherent conducting organometallic polymer. For hydrogen-doped *poly*-MTO samples $\{H_{0.5}[(CH_3)_{0.92}ReO_3]\}_\infty$ obtained by polymerization in an aqueous solution a moderately high electrical dc resistivity of 6 mΩ cm at room temperature and a Pauli-like high-temperature magnetic susceptibility of 70×10^{-6} emu/mol was found in earlier studies.[1,2] The increase of the susceptibility with decreasing temperature was ascribed to an antiferromagnetic coupling mechanism and the conductivity was explained by the presence of demethylated Re atoms (approximately 8% of all Re atoms are lacking a methyl group) and acidic hydrogen atoms which formally act as a source of itinerant electrons of the transition-metal oxide lattice.[3] The results of band-structure calculations employing the extended Hückel theory were interpreted by Genin *et al.*[4] such that these demethylated Re atoms, which formally represent $Re^{VI}(d^1)$ sites, are effectively oxidized and their valence electrons are transferred to the band system. Only a minor part of these electrons (0.05% Re atoms[5]) remains located at the metal sites which are in the following treated as Re(d^1) centers. These paramagnetic centers build up a two-dimensional (2D), diluted metal-oxide spin system in a metal-like matrix. These experiments to enhance the electronic conductivity of *poly*-MTO by employing the organic donor species tetrathiafulvalene (TTF) led to an amazing result: a crossover from a metallic to insulating behavior with increasing TTF contributions.[5]

In a recently published paper[6] it is observed that the resistivity of *poly*-MTO at low temperatures and in high magnetic fields within the $\{ReO_2\}_\infty$ planes resembles the behavior of ρ of the $\{CuO_2\}_\infty$ planes in Zn-doped high-T_c superconductors, e.g., $YBa_2CuO_{7-\delta}$ (Ref. 7) and $La_{1.85}Sr_{0.15}CuO_4$ (Ref. 8). At low temperatures a logarithmic divergence of $\rho\sim\ln(1/T)$ over an extended temperature range is observed, followed by a square root behavior ($\rho\sim\sqrt{T}$). In this insulating regime, a positive, increasing magnetoresistance (MR) is found. In the case of Zn-doped high-T_c superconductors the scattering centers are established by nonmagnetic Zn atoms within the antiferromagnetic spin-correlated $\{CuO_2\}_\infty$ planes,

 ©2006 The American Physical Society

whereas the scattering centers of *poly*-MTO reflect the inverse situation: magnetic Re(d^1) centers are placed in nonmagnetic $\{ReO_2\}_\infty$ planes.

Many high-T_c cuprates feature this logarithmic divergence of the resistivity at low temperatures, when superconductivity is entirely suppressed by, e.g., applied magnetic fields[7,9,10] or point defects, such as Zn or Li impurities[7,8,11] or oxygen and copper vacancies[12] (for a short overview, see Ref. 13). Up to now various models have been proposed to describe the $\ln(1/T)$ behavior in the insulating regime. Here we mention some of them: (i) In $Tl_2Ba_2CuO_{6+\delta}$ the defect scattering is purely elastic and is accounted for by a 2D weak localization theory.[12] (ii) A Kondo-like scattering is proposed for the underdoped $YBa_2CuO_{6.6}$ controlled by electron irradiation or for the magnetic properties of $YBa_2CuO_{6.7}$ induced by spinless defects such as 2.7% Zn.[12] (iii) Varma suggested for single layer Bi compounds a temperature-dependent impurity scattering time in a marginal Fermi liquid.[14] (iv) A conventional electron-electron interaction in a 2D disordered system[15] is also valid to describe the electronic situation for different types of cuprates.[9,16] However, there is still no consensus about this issue. In this respect *poly*-MTO may be a promising model system to shed more light on the multifarious discussion about the electron-scattering mechanism in cuprates.

In this paper the exceptional 2D character of the structure as well as of the charge-carrier transport of *poly*-MTO is consistently revealed by density-functional theory (DFT) calculations, x-ray diffraction, IR studies, specific heat, and electrical resistivity measurements. For intercalated *poly*-MTO we present a phase diagram separating the metallic phase ($d\rho/dT>0$) from the insulating one ($d\rho/dT<0$), taking into account guest molecules such as the organic donor molecules TTF, and the inorganic acceptor compound SbF_3. Furthermore, ESR results support the presence of spatially localized electrons as revealed by the presence of Re(d^1) centers.[6] In addition, we present a detailed analysis of the temperature dependence of the resistivity data in the insulating regime in comparison to the Zn-doped high-T_c superconductor $La_{1.85}Sr_{0.15}CuO_4$.[8] In particular, we will show that the Altshuler-Aronov correction[15] (disorder enhanced electron-electron interaction) works very well in describing the low-temperature resistivity data for both, *poly*-MTO and Zn-doped $La_{1.85}Sr_{0.15}CuO_4$.

II. PREPARATION AND CHARACTERIZATION

A. Synthesis

As a starting material for *poly*-MTO we prepared methyltrioxorhenium (MTO) in the following way:[17] Rhenium powder (10.43 g, 56.0 m mol) was suspended in 10 ml of water. Under cooling employing an ice-water bath and efficient stirring, a total of 100 ml of 35% H_2O_2 was added in five portions within 2 h. After stirring for 1 h at room temperature, the mixture was heated to 80 °C for 2 h and then cooled to room temperature. A solution of $AgNO_3$ (10.0 g, 58.8 m mol) in 20 ml of water was then added. After stirring for 30 min, the precipitate was filtered off, washed with water (2 times 40 ml) and diethylether (2 times 60 ml), and dried for 5 h at room temperature and 0.2 mbar. The yield of $AgReO_4$ was 17.9 g (89%). The dry $AgReO_4$ was dissolved in 180 ml of dry acetonitrile under nitrogen, and 13.7 ml (108.4 m mol) of trimethylchlorosilane were added, followed by tetramethyltin (7.5 ml, 54.0 m mol). Stirring under nitrogen was continued for 16 h. The precipitate was then filtered off under nitrogen with a G3 glass filter and washed with acetonitrile (60 ml). The solvents were removed from the combined filtrates at 0.2 mbar at room temperature, and the semisolid residue was washed with hexane (2 times 60 ml). The solid residue was purified by sublimation at 0.2 mbar/55 °C (oil bath temperature). The sublimation was repeated once to obtain pure material, showing no impurities in the ^{1}H-NMR spectrum, giving correct C, H, Re elemental analysis, and having a melting point of 106 °C. The yield was 9.06 g (65% rel. Re metal).

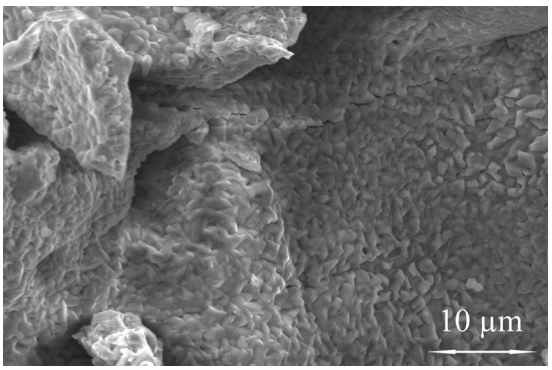

FIG. 1. Scanning electron microscope micrograph of *poly*-MTO microcrystalline grains.

For the synthesis of *poly*-MTO, two methods have been established. The first consists in dissolving MTO (CH_3ReO_3) in water under stirring at 80 °C for two days.[18] However, this is neither applicable to the intercalation of TTF since this compound is not soluble in water, nor to other reactive intercalates which often decompose in the presence of water. A second method for *poly*-MTO synthesis has, therefore, been developed which is based on autopolymerization of MTO in the melt (melting point of pure MTO: 106 °C). The resulting polymer is a golden colored solid compound. A scanning electron microscope image of *poly*-MTO is depicted in Fig. 1 indicating an assemble of microcrystalline grains with typical diameters between 0.7 and 1.3 μm which stick together.

The second technique allows for convenient and efficient intercalation of a variety of organic, organometallic and inorganic guest species. Thus, finely ground mixtures of MTO and the intercalates (TTF, BEDT-TTF, SbF_3) in appropriate ratios are heated in sealed ampoules at 120 °C or, more conveniently, in closed screw cap glasses during two days (three days for the samples with BEDT-TTF). The products were washed with an appropriate solvent to remove unreacted starting materials (hexane for TTF, THF for BEDT-TTF, and toluene for SbF_3), and dried under argon. The samples were analyzed for their composition by an elemental analysis (C, H, S, using an Elementar Vario EL III apparatus), and inductively coupled plasma–OES techniques (Re, S, Sb, with a Varian Vista MPX instrument). From the

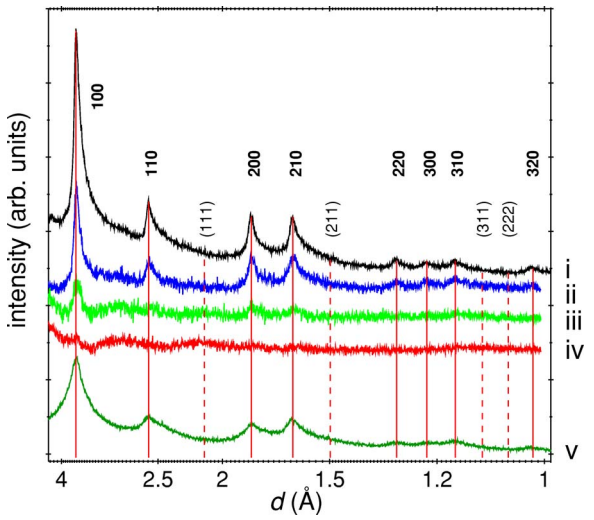

FIG. 2. (Color online) X-ray powder diffraction patterns (Cu K_α and Mo K_α radiation) (Ref. 21) of selected samples: (i) Parent compound *poly*-MTO; (ii) and (iii) *poly*-MTO intercalated by 9% and 29% TTF, respectively; (iv) *poly*-MTO intercalated by 25% BEDT-TTF, and (v) by 1.1% SbF_3. The systematic absence of reflections *hkl* with $l \neq 0$ indicates a layered structure without 3D ordering for all samples.

analytical data, the formula and the molecular weight were calculated as $(CH_3)_yReO_3(\text{intercalate})_x$, taking into account that *poly*-MTO shows a reduced content of methyl groups ($y \leqslant 0.92$). The intercalated samples (formulated as *poly*-MTO+x% TTF) prepared by this way form bronze-colored solids for low TTF concentrations ($x < 40$) and almost black powders for higher intercalation ratios. Whereas pure *poly*-MTO and its intercalated SbF_3 derivatives exist as bronze-colored grains, the BEDT-TTF intercalated samples are available solely as black powders.

B. Structural characterization

All samples have been characterized by x-ray powder diffractometry. The diffraction pattern of these *poly*-MTO samples exhibits two remarkable features: First, all observed Bragg reflections of the various samples can be indexed by the same cubic lattice parameter $a=3.66(1)$ Å. This lattice parameter is related but significantly different from those reported for the cubic inorganic oxides ReO_3 ($a=3.748(1)$ Å) (Refs. 1 and 19) and $Re_{1-x}W_xO_3$ [$a=3.7516(2)$ Å; $x=0.25$].[20] We note further the systematic absence of reflections *hkl* for $l \neq 0$ (see curve *i* in Fig. 2, dashed lines). This is a strong evidence for periodic ordering in these *poly*-MTO samples to occur exclusively in two dimensions.

A second hint for the presence of a layered structure without 3D ordering is given by the asymmetry of the reflection profiles which shows a slow decay of Bragg intensity in the direction of decreasing *d* values (cf. 100 and 110 reflections in Fig. 2). This peak shape asymmetry is a well-known indicator for layered compounds displaying a turbostratic or 00*l* defect stacking. The reciprocal space construction for the resulting 2D diffraction pattern consists of spread diffuse 00*l* rods parallel to the *c* axis (stacking direction) which cause the smooth decay of the Bragg intensities of each *hk*0 reflection with an increasing diffraction angle θ or decreasing *d* values.[2]

The observed diffraction pattern for *poly*-MTO is, therefore, in accord with the 2D space group *p*4*mm* and a square unit cell. Hence, an idealized structural model for *poly*-MTO can be derived from the inorganic parent compound ReO_3 (space group $Pm\bar{3}m$) by adopting its perovskite structure in two dimensions in the form of $\{ReO_2\}_\infty$ layers. Complementing the coordination environment of the Re atom by one methyl (CH_3) and one oxo (O) group led to a layered network of CH_3ReO_5 octahedra displaying an averaged Re-Re separation of about 3.67 ± 0.02 Å.

Samples intercalated by the acceptor SbF_3 show no significant change of the 2D character. The intercalation by TTF and BEDT-TTF preserves the 2D structural character. However, the periodicity within this structure becomes reduced with increasing donor concentrations resulting in amorphouslike x-ray patterns (see, for selected samples, curves ii-v in Fig. 2).

For a closer investigation of the structure of these layers the geometry of several two-dimensional models of *poly*-MTO were fully optimized using the density functional theory (DFT) methods with periodic boundary conditions as implemented in the GAUSSIAN03 program package.[22] The PBEPBE functional in combination with the CRENBL basis-set and an averaged relativistic effective core potential for Re and a standard 3-21G* basis-set for C, H, and O was used throughout.[23,24] Auxiliary density fitting functions were generated employing the standard algorithm implemented in GAUSSIAN03.[22] The translational asymmetric unit was in each case set up as $[\{(CH_3)ReO_3\}_3ReO_3]_\infty$ to account for the deficiency of methyl groups. However, this leads to a ratio C:Re of 0.75 in our model which is somewhat below the experimental value of about 0.92 found by the elementary analysis. The models were tested for different orientation patterns of the methyl groups, the one leading to the lowest total energy, labeled *model I*, is shown in the lower panel of Fig. 3. It should be mentioned that this model adopts the layered structure of the transition-metal oxide tungstite, $WO_3 \cdot H_2O$, when replacing the methyl ligands by water molecules.[25] We note that the close structural analogy between tungstite and *poly*-MTO could be used to employ both compounds as sol-gel precursors for the synthesis of mixed $Re_{1-x}W_xO_3$ ceramics by *chimie douce* methods.[20]

The calculated Re—Re distance of 3.79 Å (average value) is in good agreement with the distance of 3.67 Å found in the x-ray diffraction pattern. Starting from an approximately octahedral coordination environment of the Re atoms a significant distortion of the idealized geometry is found. This is indicated by average O—Re—O angles of 169.3° and 154.9° in the $\{ReO_2\}_\infty$ plane for the CH_3ReO_3 and the ReO_3 fragment, respectively. The C—Re—O angle clearly deviates from the ideal angle of 180° in the octahedral case and is reduced to 149.7°. In addition to the nonplanarity of the $\{ReO_2\}_\infty$ layer, there also exist two different Re—O bond distances (1.82 and 2.05 Å, average values) for the methylated rhenium atoms. Each of these Re atoms thus exhibits two short and two longer Re—O bonds inside the

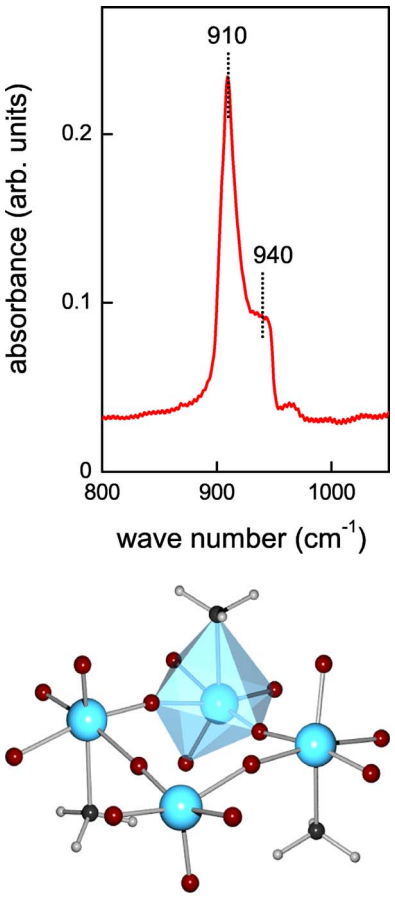

FIG. 3. (Color online) Top: The IR spectrum of *poly*-MTO exhibits an asymmetric (910 cm^{-1}) and a symmetric (940 cm^{-1}) Re—O stretching mode which clearly deviate from the corresponding values in the monomer MTO [$\nu_{as}(ReO_3)$: 955 cm^{-1}; $\nu_s(ReO_3)$: 1000 cm^{-1}]. Bottom: DFT optimized structural *model I* of *poly*-MTO (see also Fig. 15).

$\{ReO_2\}_\infty$ plane. This effect is somewhat less pronounced for the ReO_3 moiety, for which Re—O bond distances of 1.81 and 1.96 Å inside the $\{ReO_2\}_\infty$ plane are found.

C. IR spectroscopy

Infrared spectra were recorded at room temperature with a Bruker Fourier-transform spectrometer IFS66v/S. Transmission spectra of the samples pressed into KBr pellets were collected in the midinfrared range from 500 to 5000 cm^{-1}. The upper panel of Fig. 3 shows the dominant vibrational double mode at 910 and 940 cm^{-1}. Most likely, these two bands arise from the two Re-O stretching modes [asymmetric (as) and symmetric (s)], which were found for solid state MTO at 959 cm^{-1} [$\nu_{as}(ReO_3)$] and 998 cm^{-1} [$\nu_s(ReO_3)$] prepared in CsI pellets.[26] This is in fine agreement with room-temperature KBr pellet spectra of our MTO precursor material, which display these two modes at 955 and 1000 cm^{-1}, respectively.

The shift of the vibrational excitations to lower energies for the polymerized material measured under the same conditions indicates a weakening of the Re—O bonding in the terminal Re═O groups due to trans-influence of the CH_3 group. This is in line with the 2D structural DFT model discussed above (see Fig. 3) which shows an elongation of the Re═O bond in *poly*-MTO by about 0.024 Å relative to CH_3ReO_3.

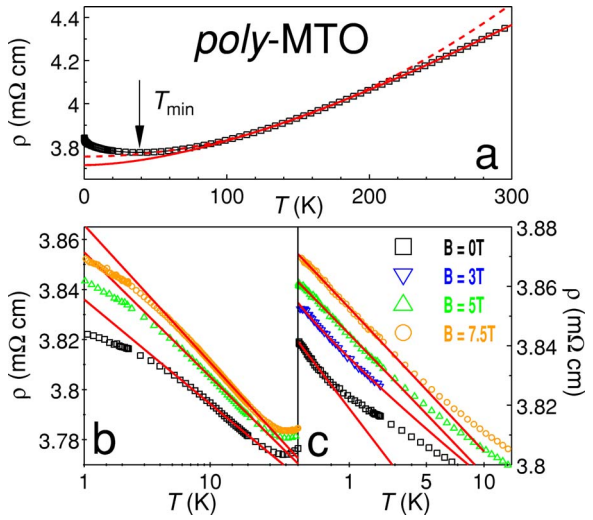

FIG. 4. (Color online) (a) Resistivity $\rho(T)$ of *poly*-MTO on a linear scale below 300 K. The dashed line presents a fit according to $\Delta\rho(T) \propto T^2$ for 100 K $> T >$ 200 K, the solid line is a fit $\Delta\rho(T) \propto T^2 \ln(T_F/T)$ for $T >$ 90 K (see text). (b) A semilogarithmic plot of $\rho(T)$ in various magnetic fields. The solid lines are logarithmic fits between 5 and 30 K. (c) Resistivity $\rho(T)$ plotted vs square root T below 10 K.

III. EXPERIMENTAL RESULTS

A. Resistivity

Resistance measurements were performed by a four-point low-frequency ac method below 300 K over four temperature decades. For the determination of the resistivity of *poly*-MTO one has to take into account a rough estimate of the nonuniform sample shape causing a relative error bar of 30% for the residual resistivity.

In Fig. 4(a) the resistivity of *poly*-MTO is plotted vs temperature. The temperature dependence of the resistivity clearly exhibits a minimum at about T_{min}=38 K. Above 38 K the resistivity increases monotonically and nonlinearly with increasing temperature indicating metallic behavior. In order to identify the dominating scattering mechanisms we analyzed the data in terms of a power law.[27] A least squares fit according to $\rho(T)=\rho_0+A_{ee}T^2$ between 100 and 200 K [dashed line in Fig. 4(a)] reveals a residual resistivity ρ_0 =3.76 mΩ cm and an electron-electron scattering amplitude $A_{ee}=7.9\times10^{-3}$ $\mu\Omega$ cm K^{-2}. However, above 200 K and below 80 K the fit deviates substantially from the data.

The absolute value of A_{ee} is enhanced by a factor of 10^6 compared with the value of simple metals,[28] but is of the same order as found for high-T_c superconductors.[29] This strong enhancement of the electron-electron scattering amplitude is most likely due to a significant anisotropy in our sample. If the 2D nature of *poly*-MTO—as derived from

x-ray measurements—is the origin of such a large enhancement of A_{ee}, then we have to take into account the relaxation rate $(1/\tau_{ee})$ for quasiparticles of a 2D electron system,[30] which can be expressed as:

$$\frac{1}{\tau_{ee}} \simeq \left(\frac{T}{T_F}\right)^2 \ln\left(\frac{T_F}{T}\right). \quad (1)$$

The resistivity can therefore be written as

$$\rho(T) = \rho_0 + K\left(\frac{T}{T_F}\right)^2 \ln\left(\frac{T_F}{T}\right), \quad (2)$$

where K is a constant. The solid line in Fig. 4(a) is a fit according to Eq. (2) over the whole temperature range above 90 K, leading to a residual resistivity $\rho_0 = 3.75$ mΩ cm and a Fermi temperature $T_F \simeq 2300$ K. As can be clearly seen, the fit reproduces the data convincingly, suggesting that the high-temperature resistivity of *poly*-MTO is actually consistent with Fermi-liquid theories of electron-electron scattering in pure 2D metals.[30,31] The relatively low value of the Fermi temperature may be due to the low charge-carrier concentration and is comparable to values observed for high-T_c superconductors [e.g., for the classical hole superconductor $YBa_2CuO_{7-\delta}$ (Ref. 32) or for the electron-doped superconductor $Nd_{1.85}Ce_{0.15}CuO_4$ (Ref. 29)]. The nonlinear temperature dependence of ρ excludes a significant amount of electron-phonon interaction. From the latter one would expect a linear temperature dependence above a characteristic temperature $T^* \approx 0.3\Theta_D$; for *poly*-MTO $\Theta_D(2D) = 206$ K and $\Theta_D(3D) = 66$ K (see Ref. 5).

Figures 4(b) and 4(c) illustrate the low-temperature resistivity in more detail. Below 30 K a $\ln(1/T)$ divergence over one decade of T is observed [Fig. 4(b)], and at lowest temperatures a power-law dependence is detected, $\Delta\rho \propto T^\alpha$, with $\alpha \approx 0.5 \pm 0.1$ [Fig. 4(c)]. It should be mentioned that with increasing magnetic field the temperature range of the square root behavior is expanded. In a recent paper[6] it is suggested that the origin of the $\ln(1/T)$ and $\sqrt{T}$ behaviors may be due to an additional resistivity contribution related to an electron-electron scattering in the presence of a random disorder potential known as the Altshuler-Aronov[15] correction. This will be discussed in more detail in Sec. IV.

In order to increase the concentration of conducting electrons we performed controlled intercalation of donor and acceptor specimens. The temperature-dependent electrical resistivity $\rho(T)$ of *poly*-MTO intercalated with the organic donor molecule TTF and the inorganic acceptor compound SbF_5 is plotted in Fig. 5(a) for various concentrations normalized to $\rho(300\ \text{K})$ of *poly*-MTO.[33] None of the intercalated compounds exhibits a significant enhancement of the metallic behavior. The residual resistivity increases with increasing TTF concentrations, while it is almost constant for the SbF_5 samples. However, all $\rho(T)$ curves clearly exhibit a crossover from metallic to insulating behavior at T_{min}.

The solid (TTF) and dashed (SbF_5) lines are fits taking into account Eq. (2) plus an additional $\ln(1/T)$ term describing the temperature dependence of $\rho(T)$ below T_{min}. The fits reproduce the data convincingly using a Fermi temperature of $T_F = (2500 \pm 500)$ K. It is conspicuous that for all samples

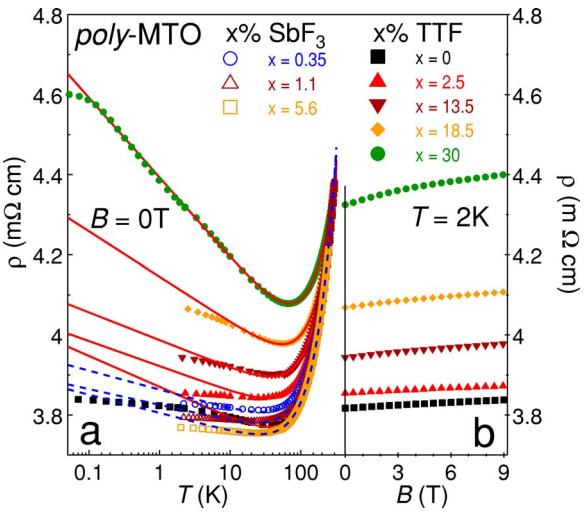

FIG. 5. (Color online) (a) $\rho(T)$ of *poly*-MTO intercalated with the organic donor species (TTF) and the inorganic acceptor SbF_5. Note that the resistivity curves of all samples are normalized to $\rho(300\ \text{K})$ of *poly*-MTO since the complex shape of the samples prevents a geometrical modeling of their morphology. The solid (TTF) and dashed (SbF_5) lines are fits to the data, discussed in the text. (b) The magnetoresistance of the TTF intercalated samples at $T = 2$ K.

the 2D character of the electron system is preserved. Furthermore, the logarithmic divergence below T_{min} becomes more pronounced with increasing TTF concentration, whereas it remains independent of concentration for the acceptor specimens doped with SbF_5. These different types of behavior between the donor- and acceptor-intercalated compounds are in line with the results of the magnetization measurements indicating that the logarithmic temperature dependence has its origin in the amount of $Re(d^1)$ centers (Sec. III B, Table I). For all TTF-intercalated samples a positive, nearly linearly increasing magnetoresistance was found in this insulating regime at $T = 2$ K [Fig. 5(b)]. The same phenomenon was also observed for pure *poly*-MTO.[6]

A temperature T_{min} was designated as transition temperature between the metallic $(d\rho/dT > 0)$ and the insulating $(d\rho/dT < 0)$ phase [see Fig. 4(a)] to generate a preliminary *phase diagram* shown in Fig. 6 as a function of TTF and SbF_5 concentrations. Here the SbF_5 concentration is furnished with a negative sign to distinguish acceptor character from donor behavior (positive sign). The concentration dependence of T_{min} of the SbF_5 intercalated specimens is rather weak and therefore SbF_5 does not seem to be a suitable compound to follow the extrapolated phase boundary (solid line in Fig. 6). This phase diagram is similar to that found in various high-T_c-superconductors[10,34,35] indicating that *poly*-MTO and its intercalated specimens may be a promising starting material for the design of superconducting organometallic polymers.

B. Susceptibility and magnetization

Magnetization and susceptibility are excellent measures to get more information about the partially localized electrons

TABLE I. Localized and itinerant moments evaluated from susceptibility and magnetization measurements of *poly*-MTO and its intercalated hybrids with TTF, BEDT-TTF, and SbF_3. Note that χ_0^{sus} and χ_0^{mag} are given in units of 10^{-6} emu/mol.

	x (%)	$\chi_0^{sus}/\chi_0^{mag}$	$\mu_{eff[exp]}$ (μ_B/f.u.)	$1/n$	μ_B/m_S
poly-MTO		110/120	0.039	2000	2300
TTF	2.5	102/126	0.065	689	724
	4	90/129	0.084	422	440
	9	92/149	0.112	240	263
	13.5	72/155	0.142	148	161
	18.5	71/167	0.156	125	135
	30	61/164	0.161	115	124
BEDT-TTF	11.5	68/169	0.163	112	103
	25	58/145	0.206	70	64
	36	75/155	0.223	62	62
SbF_3	0.35	120/114	0.060	833	1000
	1.1	87/110	0.049	1250	1600
	5.6	97/120	0.063	760	926

causing a certain amount of paramagnetic $Re^{VI}(d^1)$ centers. We noted before that these electrons as well as the itinerant electrons in the conduction band originate from the loss of 8% of the methyl groups in *poly*-MTO. This section focuses on the role of these additional electrons originating from this demethylation of Re and tries to clarify whether these electrons are localized or itinerant in *poly*-MTO and its intercalated systems. A superconducting quantum interference device (SQUID) served for the determination of the magnetization m from 1.9 K up to 300 K in magnetic fields up to 7 T.

For pure *poly*-MTO the magnetic dc susceptibility $\chi(T)$

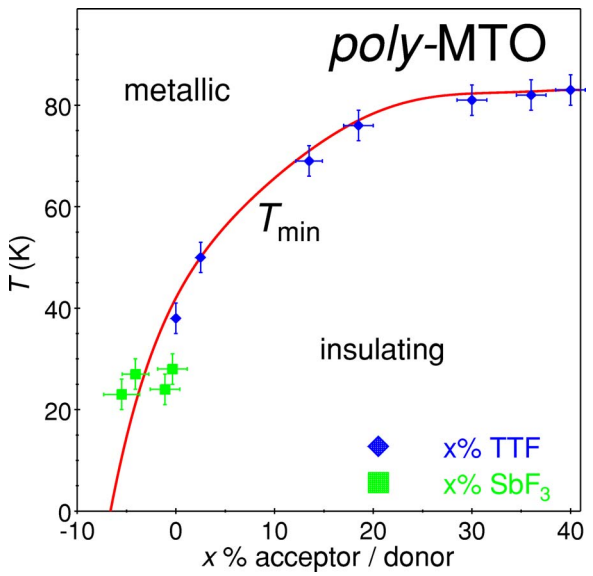

FIG. 6. (Color online) Phase diagram of *poly*-MTO intercalated with x% of the donor TTF and acceptor SbF_3. The line represents the temperature T_{min} determined from the resistivity data in Fig. 5.

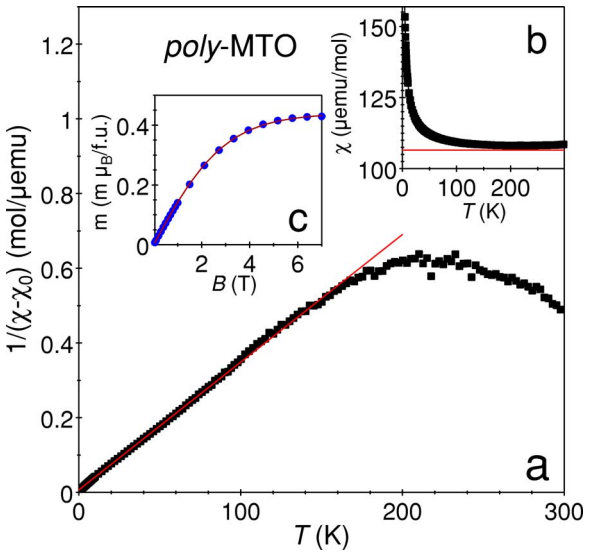

FIG. 7. (Color online) (a) Inverse magnetic susceptibility of *poly*-MTO measured in an applied magnetic field of $B=1$ T. The solid line is a fit of the modified Curie-Weiss–type behavior. (b) The magnetic dc-susceptibility ($\chi=m/B$). (c) The magnetic field dependence of the magnetization. The solid line follows a Brillouin function for a d^1 moment (see text).

$=m(T)/B$ is pictured in Fig. 7(b). Due to the small susceptibility values the data are corrected by the core diamagnetism $\chi_{dia}^{Langevin}=-69\times10^{-6}$ emu/mol.[36] It is interesting to note that above 100 K the susceptibility increases with increasing temperature, while below 100 K a paramagnetic contribution emerges and gets dominant. The unusual high-temperature behavior, which is present just in the metallic region as revealed by the resistivity measurements, may be interpreted by a reduction of the itinerant electron concentration with decreasing temperature. Another reason could be that the crystal-field splitting of the Re d orbital manifold is small enough to allow for non-negligible Van-Vleck contributions to the susceptibility.

Below 70 K the susceptibility can be well described by a modified Curie-Weiss type behavior, $[\chi(T)-\chi_0^{sus}]=C/(T-\Theta_{CW})$ with a marginal itinerant contribution $\chi_0^{sus}=110\times10^{-6}$ emu/mol, yielding an average Pauli susceptibility $\chi_P=3/2\chi_0^{sus}=165\times10^{-6}$ emu/mol [cf. Fig. 7(a) and Table I].[36]

The vanishing paramagnetic Curie-Weiss temperature $\Theta_{CW}=0$ K indicates that no correlations between the magnetic moments of the residual localized electrons at the $Re(d^1)$ centers are present. The effective paramagnetic moment $\mu_{eff}=39\times10^{-3}\mu_B$ (Table I) obtained from the Curie constant C is smaller than expected for $Re^{VI}(d^1)$ ions by two orders of magnitude. Assuming that only integer fractions of $Re^{VI}(d^1)$ ions exist, the small effective moment indicates that roughly one $Re^{VI}(d^1)$ center per 2000 Re atoms is present. The inverse of that virtual Re^{VI} concentration $1/n=\mu_{eff[Re\ d^1]}^2/\mu_{eff[exp]}^2$ (with $\mu_{eff[Re\ d^1]}=1.73\mu_B$) is listed in Table I.

In Fig. 7(c) the field dependence of the magnetization $m(B)$ after subtraction of the core diamagnetism[36] and the

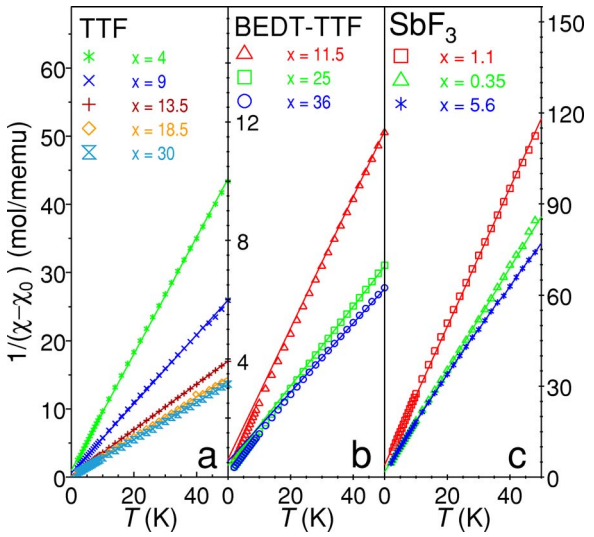

FIG. 8. (Color online) Inverse magnetic susceptibility vs temperature in an applied field of 1 T for (a) *poly*-MTO+x% TTF, (b) *poly*-MTO+x% BEDT-TTF, and (c) *poly*-MTO+x% SbF_3. All lines are fits of the modified Curie-Weiss–type behavior.

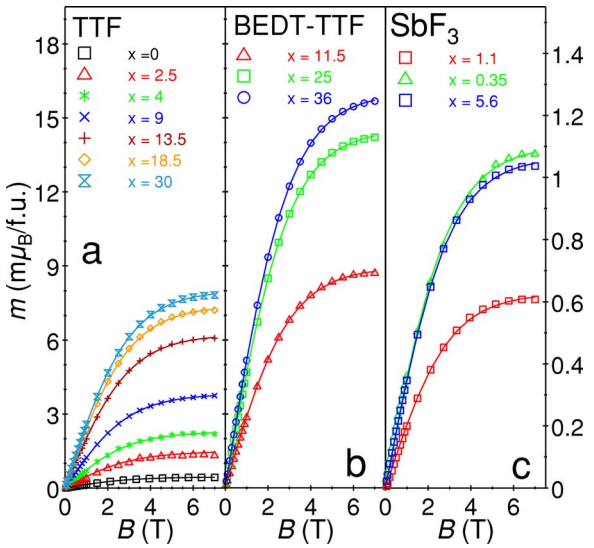

FIG. 9. (Color online) Magnetic field dependence of the magnetization at 2 K for (a) *poly*-MTO+x% TTF, (b) *poly*-MTO+x% BEDT-TTF, and (c) *poly*-MTO+x% SbF_3. All lines are fits based on Brillouin functions (see text).

itinerant electron contribution (χ_0^{mag}) at 2 K is displayed. The solid line obeys a Brillouin function taking into account an Re(d^1) electron configuration with a quenched orbital moment (L=0) using χ_0^{mag} and the saturation magnetization (m_s) as fit parameters. This fit led to nearly the same amount of 1/2300 localized Re(d^1) centers per formula unit as obtained from the susceptibility measurement (cf. Table I).

The inverse susceptibility of TTF-, BEDT-TTF- and SbF_3-intercalated *poly*-MTO samples below 50 K is plotted vs temperature for various concentrations in Fig. 8. In the high-temperature regime (not displayed) the weakly intercalated samples follow the same unusual temperature dependence as *poly*-MTO but in a temperature range which shifts towards higher temperature with increasing concentration. The fits of the modified Curie-Weiss law (solid lines) match the data very well. The resulting values of $\mu_{eff[exp]}$ and χ_0^{sus} are listed in Table I, using the same calculation procedure as described for pure *poly*-MTO.

It can be seen from Table I that with increasing donor concentration the itinerant contribution (χ_0^{sus}) decreases while the effective magnetic moment ($\mu_{eff[exp]}$) increases, mirroring the cumulative amount of localized electrons as reflected by the presence of $Re^{VI}(d^1)$ centers. As a consequence, the number of Re atoms which share one spin moment ($1/n$), decreases strongly with increasing x except for SbF_3.

This is also supported by the magnetization measurements $m(B)$ displayed in Fig. 9. The solid lines are fits, following the Brillouin function for a Re(d^1) electron configuration, using the saturation magnetization m_s and χ_0^{mag} as fit parameters. The enhancement of χ_0^{mag} by a factor of approximately 2 in comparison with χ_0^{sus} (cf. Table I) may be due to the crossover behavior from a 2D to a 3D system at about 2 K as revealed by the resistivity measurements (Sec. III A). For TTF and BEDT-TTF one μ_B divided by m_s (note that m_s has the unit of μ_B) equals roughly $1/n$ derived from the susceptibility data at high temperatures. Therefore, both $\chi(T)$ at elevated temperatures and m_s at 2 K, report independently the increasing local character of the electrons at the Re^{VI} ions introduced via intercalation. However, for the SbF_3-intercalated samples this tendency could not be observed within the error bars.

In spite of the increasing carrier localization with increasing donor concentration no magnetic correlations are observed as indicated by the vanishing paramagnetic Curie-Weiss temperature (Θ_{CW}=0 K). These results are plausible taking into account the mean distance $d_{Re^{VI}-Re^{VI}}$ of the remaining local Re(d^1) centers within the planes (e.g., for pure *poly*-MTO, $d_{Re^{VI}-Re^{VI}} \approx 140$ Å; for x=30% TTF, $d_{Re^{VI}-Re^{VI}} \approx 40$ Å). This large separation of the local magnetic moments is still too large to form magnetic correlations.

In a recent paper we suggested that also the magnetic field may represent a tuning parameter for an additional localization scenario from which the positive magnetoresistance in pure *poly*-MTO originates.[6] However, this effect is also observed in *poly*-MTO samples intercalated by 2.5% TTF. In Fig. 10(a) the magnetization m divided by the applied magnetic field B is plotted vs temperature. Again, the solid lines are Brillouin fits. The amount of Re(d^1) centers, formally deduced from these fits, is pictured in Fig. 10(b). In Fig. 10(c) the relative increase of the magnetoresistance of *poly*-MTO at 100 mK is plotted vs the amount of Re(d^1) centers for various fields. Assuming that the magnetic moment has its origin only in the amount of the Re(d^1) centers this linear behavior is a clear evidence that with increasing magnetic field the amount of localized electrons and thus the amount of Re(d^1) centers increases linearly.

C. ESR analysis

To get more detailed information concerning the origin of the remaining local electrons, electron spin resonance (ESR)

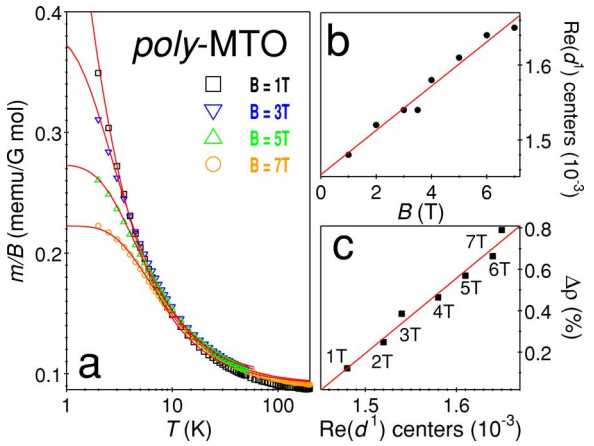

FIG. 10. (Color online) (a) m/B of *poly*-MTO in several external magnetic fields. The solid lines are Brillouin fits for a Re(d^1) configuration. (b) The amount of Re(d^1) centers deduced from the fits vs B. (c) Percentage increase of the resistivity with magnetic field vs the amount of Re(d^1) centers.

measurements were performed. The ESR measurements were carried out at X-band frequencies (9.4 GHz) with a Bruker ELEXSYS E500-CW spectrometer using a continuous helium gas-flow cryostat (Oxford Instruments) for temperatures $4.2\ \mathrm{K} \leqslant T \leqslant 300\ \mathrm{K}$. To avoid the influence of the skin effect due to the conductivity,[37] the polycrystalline samples have been powdered to grains as small as possible ($<40\ \mu$m) and immersed in paraffine. Only for the pure *poly*-MTO sample the grain size was still not smaller than the skin depth and the influence of dispersion was visible in the ESR spectra. For all TTF and BEDT-TTF intercalated compounds, however, the skin effect was negligible.

Electron spin resonance detects the power P absorbed by the sample from the transverse magnetic microwave field as a function of a static magnetic field B. The signal-to-noise ratio of the spectra is improved by recording the derivative dP/dB using a lock-in technique with field modulation. Figure 11(a) shows a spectrum of *poly*-MTO intercalated with 30% TTF which is characteristic for all TTF and BEDT-TTF-intercalated samples as well. All samples exhibit a broad absorption band consisting of several broad lines with individual linewidths larger than 50 mT and a sharp resonance [cf. Fig. 11(b)] at a resonance field of 0.334 T corresponding to $g=\hbar\omega/\mu_B B=2.004$ with a linewidth of approximately 1 mT. The linewidths and line positions of the spectra are independent of the temperature, but their intensities which reflect the corresponding spin susceptibilities, χ_{ESR}, follow a Curie law as, e.g., indicated in Fig. 11(c) for the narrow line which can easily be detected up to high temperatures. This result is in good agreement with dc susceptibility data (Fig. 8).

To identify the ESR probes responsible for the observed spectrum we measured $As(C_6H_5)_4ReNCl_4$ as a reference compound,[38] which contains Re in oxidation state +VI with electronic configuration $5d^1$ as the only magnetic center. Its ESR spectrum is displayed as a dotted line in Fig. 11(a). One observes a similar broad absorption band with characteristic lines like those in the *poly*-MTO samples but without the

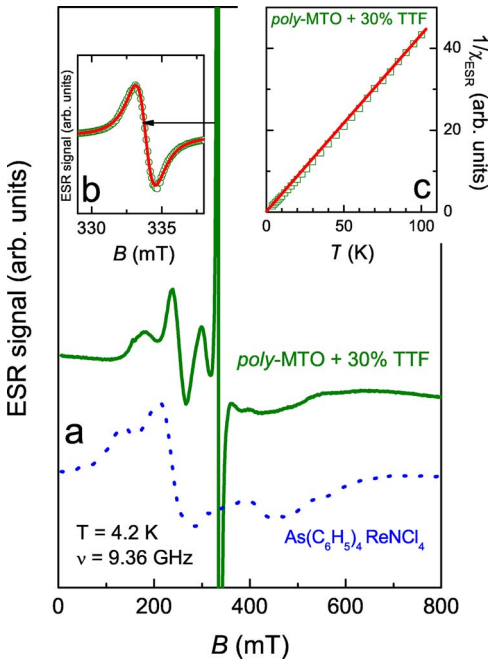

FIG. 11. (Color online) (a) A typical ESR resonance spectrum of an intercalated *poly*-MTO sample (solid line). The dotted line exhibits the spectrum of the reference compound $As(C_6H_5)_4ReNCl_4$. (b) The narrow signal at 0.334 T corresponds to a g factor of 2. The solid line is a Lorentz fit to the data. (c) The calculated intensity of the Lorentz curve follows a Curie law (solid line).

pronounced sharp resonance at $g=2$. This broad absorption band results from the hyperfine interaction of the Re(d^1) electron spin $S=\frac{1}{2}$ with the ^{185}Re, ^{187}Re nuclear spin $I=\frac{5}{2}$. In principle, the hyperfine structure should consist of six transitions of equal intensity, but the anisotropy of the hyperfine constant gives rise to a powder average with some lines more pronounced than the others.[39] From this comparison we can immediately ascribe the broad absorption band in *poly*-MTO to d electrons, which are localized in the Re $5d$ shell. The resolved hyperfine structure corroborates the conclusion from the Curie law that there are practically no correlations between the localized electrons at the Re(d^1) sites.

At a first glance conduction electrons seem to be accountable for the observed sharp line. This can be ruled out, since its intensity follows a Curie law [see Fig. 11(c)] characteristic for localized spins in contrast to a constant Pauli susceptibility expected for itinerant electrons. In general, the intensity of the narrow line is by a factor of 10 smaller than that of the broad absorption band (Fig. 12). The intercalation dependence of the organic molecules suggests that these electrons are mainly localized at the TTF and BEDT-TTF molecules.

The quantitative comparison of the intensities of the spectra in *poly*-MTO and the reference compound allows us to estimate the number of localized electrons dependent on the degree of intercalation. In Fig. 12 the resulting local spins per Re atom are displayed vs the concentration of TTF and BEDT-TTF. We find that the intensities increase with TTF as well as with the BEDT-TTF amount. The absolute numbers are in reasonable agreement with the results obtained from SQUID measurements. For pure *poly*-MTO the spectra are

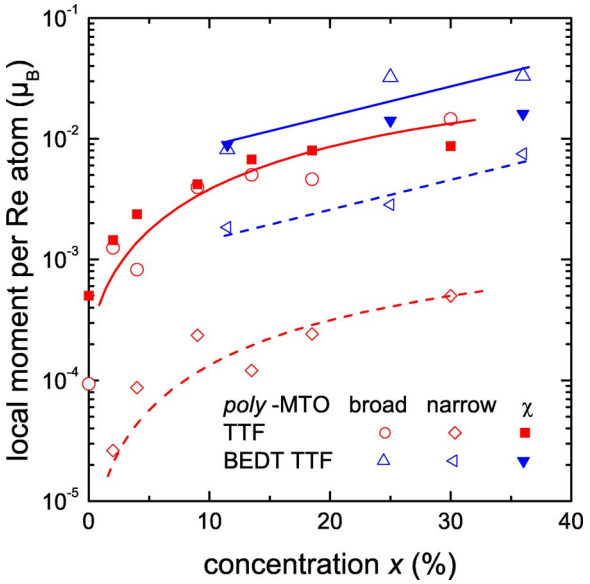

FIG. 12. (Color online) The localized moments per Re atom resulting from the calculated intensity of the broad and narrow ESR signals vs the TTF and BEDT-TTF concentration in comparison with the magnetic susceptibility findings (Table I). Note that the narrow band intensity at $g=2$ is by a factor of 10 smaller than the broadband intensity which is attributed to the $5d^1$ moment at the Re site (all lines are guides to the eye).

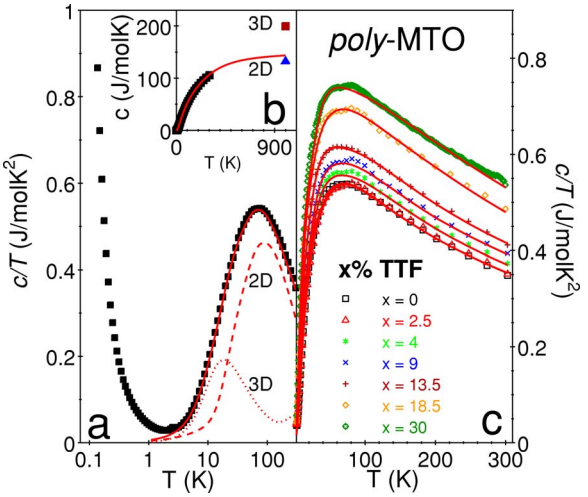

FIG. 13. (Color online) (a) Specific heat of *poly*-MTO divided by temperature vs $\log_{10} T$. The phonon contribution can be well parametrized using 75% 2D (dashed line) and 25% 3D (dotted line) terms. (b) The solid line represents an extrapolation of the calculated phonon contribution of pure *poly*-MTO. At 1000 K it is closer to the 2D Dulong-Petit limit (triangle) than to the 3D limit (square). (c) c/T vs T of *poly*-MTO+x% TTF. The solid lines are calculated phonon contributions and x is the TTF to Re ratio in %.

similar to those of the intercalated compounds, but due to a marginal amount of localized electrons they are very noisy. This is also the case for the SbF_3 intercalated samples. Here the spectra do not show any dependence on intercalation at all. So far the ESR measurements allow us to identify Re as the main localization center of the electrons. This is a convincing evidence for spatial localization of the electrons at the $Re^{VI}(d^1)$ centers which is considered as the origin of the unusual linear positive magnetoresistance in *poly*-MTO.

D. Specific heat capacity

The specific heat measurements on samples with a mass of about 3 mg were performed at temperatures ranging from 1.8 up to 300 K by means of a quasiadiabatic step heating technique in external magnetic fields up to 9 T using a physical properties measurement system from quantum design. Specific heat data were also collected at temperatures down to about 80 mK in a $^3He/^4He$ cryostat using a relaxation method.[40]

Figure 13(a) documents the molar specific heat capacity divided by temperature c/T of *poly*-MTO for temperatures $0.08\ K < T < 300\ K$. As the results cover almost four decades in temperature, for representation purposes, we display c/T vs T as a semilogarithmic plot.

Attempts to model the specific heat data by taking into account only 2D or only 3D Debye and Einstein modes fail. Alternatively, the phonon contribution can be well parametrized by a sum of 75% two- and 25% three-dimensional terms with $\Theta_D(2D)=206$ K and $\Theta_D(3D)=66$ K for the low temperature region (dashed and dotted lines in Fig. 13, respectively). The high-temperature regime is well matched using additional Einstein terms describing the vibrational modes which have a predominant molecular character. Especially the highest 3D Einstein temperature $\Theta_E(3D)=1150$ K corresponds well to the IR-active mode at 740 cm^{-1} associated with the ρ-rocking modes of the CH_3 groups of pure MTO.[26,41] In Fig. 13(b) the specific heat c of the calculated phonon contribution of *poly*-MTO is extrapolated up to 1000 K in order to compare the high-temperature value with the Dulong-Petit limit of a 2D (triangle) and a 3D (square) system. Again, the primarily 2D character of *poly*-MTO is obvious.

This 2D character of the phonon contribution is also seen for all samples intercalated with TTF. The solid lines in Fig. 13(c) display fits of the lattice contribution to the data using Debye and Einstein terms. Up to $x=30\%$ the 2D character increases slightly with decreasing Debye temperatures, yielding for 30% TTF a 2D to 3D ratio of 4 with $\Theta_D(2D)=105$ K and $\Theta_D(3D)=50$ K. Furthermore, the linear TTF concentration dependence of the high-temperature specific heat $c(300\ K)$ clearly demonstrates that TTF is completely intercalated. These results are in accordance with the fact that the TTF molecules are positioned in between the *poly*-MTO layers leading to a slightly expanded layer distance.

The specific heat results of *poly*-MTO+x% BEDT-TTF show the same tendency as found for the TTF-intercalated samples. For example, 25% BEDT-TTF also yields a 2D to 3D ratio of 4 with $\Theta_D(2D)=98$ K and $\Theta_D(3D)=40$ K and indicates a slightly stiffer lattice relative to nonintercalated samples.

The electronic contribution to the specific heat $\Delta c/T$ of *poly*-MTO was obtained by subtracting the phonon and nuclear contribution (see below) from the measured c/T value. An extrapolation of $\Delta c/T$ for $T \to 0$ K yields γ

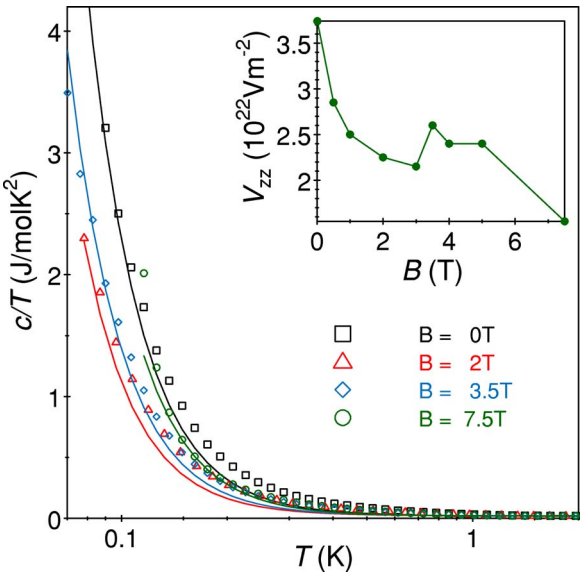

FIG. 14. (Color online) Specific heat divided by temperature vs $\log_{10} T$ of *poly*-MTO in various magnetic fields below 2 K. The strong increase of c/T below 1 K is mainly due to a nuclear magnetic and quadrupole moment indicating an internal electrical field gradient V_{zz} at the Re site which decreases with increasing magnetic field B (inset).

$\approx(13\pm2)$ mJ mol^{-1} K^{-2}, in agreement with typical values for *d*-band metals. In addition, the Wilson-ratio equals $R=\pi^2 k_B^2/(2\mu_0\mu_B^2)\chi_P/\gamma\simeq 1$ as it is expected for nonmagnetic metals. The electronic density of states of pure *poly*-MTO calculated from both, the Pauli-susceptibility $\chi_P=1.5\times\chi_0^{sus}$ and the Sommerfeld coefficient γ, yields $N(E_F)=5.2$ states/eV atom.

In order to analyze the origin of this contribution, electronic structure calculations based on density-functional theory and the local density approximation (LDA) were performed, which used the augmented spherical wave (ASW) method.[42,43] As a preliminary result, a value of $N(E_F)\approx 1$ states/eV atom was obtained.[44] According to the calculations, the density of states at the Fermi energy traces back mainly to Re(5*d*) as well as small O(2*p*) contributions. The largest 5*d* contribution stems from the Re site, which has no CH_3 group nearby.

Below 1 K the specific heat of *poly*-MTO increases considerably giving rise to a nuclear electronic Schottky effect. This effect is significantly reduced with increasing TTF intercalation.[5] We have calculated the hyperfine contributions to the heat capacity originating in zero magnetic field mainly from the quadrupole moments of ^{185}Re and ^{187}Re, and additionally from the nuclear magnetic moments of ^{1}H, ^{185}Re, and ^{187}Re in an applied magnetic field B. The fits are displayed in Fig. 14, modeling a local internal electrical field gradient V_{zz}, an average applied magnetic field, and the Zeeman splitting. We note that for zero magnetic field the enormous increase of c/T is only caused by the quadrupole moments of ^{185}Re and ^{187}Re leading to $V_{zz}=(3.7\pm0.8)\times10^{22}$ V m^{-2} (inset of Fig. 14). The large error of V_{zz} takes into account the variance of different samples and the limited accessible temperature range only including the onset of the Schottky anomaly. In contrast, the electrical field gradient of the cubic perovskite ReO_3 ($V_{zz}\simeq 0.18\times10^{22}$ V m^{-2}) is smaller by a factor of 20 than that found for *poly*-MTO. This result again clearly suggests a high anisotropy for *poly*-MTO. With increasing magnetic field V_{zz} decreases and vanishes at around $B=7$ T. Simultaneously, with increasing field the Zeeman splitting of the nuclear moment of ^{1}H becomes dominant and leads approximately to the same enhanced value of $c/T\simeq 2$ J mol^{-1} K^{-2} at 100 mK as determined only from quadrupole moments of ^{185}Re and ^{187}Re in zero field.

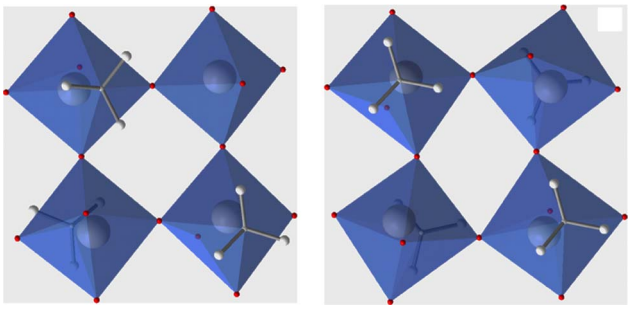

FIG. 15. (Color online) Polyhedron representation of the two-dimensional *models I* (left) and *II* (right) for *poly*-MTO (view along the *z* axis perpendicular to the $\{ReO_2\}_\infty$ planes) as obtained by DFT calculations.

The decreasing V_{zz} indicates a reduction of the electronic and structural anisotropy at the Re sites. DFT calculations on *poly*-MTO reveal that introducing an additional electron by demethylation of 25% of the Re atoms leads to a reduction of the asymmetry of the bridging Re—O bonds. A comparison of the optimized geometries of poly-MTO with one missing methyl group (*model I*; Sec. II B) and with all methyl groups present (*model II*) is depicted in Fig. 15. As a result of the presence of formal Re^{VI} centers the difference in the bond length of the bridging Re—O—Re unit inside the $\{ReO_2\}_\infty$ layers is reduced from approximately 0.4 Å (averaged value) in *model II* to approximately 0.2 Å (averaged value) in *model I*. Furthermore, the population analysis of the spin density reveals that the additional electron which was released by the demethylation process is equally distributed among the four Re atoms.[45] Thus the formal chemical reduction ($Re^{VII}\rightarrow Re^{VI}$) of one of the four Re atoms per asymmetric unit causes a clear symmetrization of the $\{ReO_2\}_\infty$ planes in *poly*-MTO. Magnetization and ESR measurements of intercalated samples reveal that a chemical reduction of Re also leads to an increase of electron localization and thus a larger amount of Re(d^1) sites. Therefore, the decrease of V_{zz} with an increasing applied magnetic field might be directly related to a magnetic field induced increase of electron localization.

IV. DISCUSSION

Now we draw our attention to the unusual temperature behavior of the resistivity of *poly*-MTO below the characteristic temperature $T_{min}\simeq 38$ K (Fig. 4). We first focus on the logarithmic increase as it is also observed in $\{CuO_2\}_\infty$ layers

of some classic cuprates known from literature (see Sec. I) and discuss possible microscopic explanations. Secondly, we will discuss the crossover (co) at a low temperature from the logarithmic temperature dependence into the square-root dependence of the resistivity at $T_{co} \simeq 1.5$ K.

Two-dimensional weak localization as a possible origin of the $\ln(1/T)$ behavior can clearly be ruled out, due to the magnetic field dependence of the resistance. A Kondo effect originated by dilute magnetic impurities might provide a reasonable explanation at the first glance, because of the small amount of the magnetic $Re^{VI}(d^1)$ centers. On the other hand, magnetic fields should suppress the Kondo effect, whereas experimentally a positive magnetoresistance is observed up to $B=7$ T [see Figs. 5(b) and 10(c)]. Another possible explanation might arise from a more exotic type of the Kondo effect: a high-temperature $\ln(1/T)$, followed by a low-temperature $\sqrt{T}$ behavior, as observed in our experiments, is predicted for systems displaying two-channel Kondo impurities.[46] The crossover temperature between $\ln(1/T)$ and $\sqrt{T}$ is expected to be specific to the microscopic realization of the Kondo impurities. However, this assumption is in clear conflict with the fact that high TTF intercalation degrees strongly reduce the crossover temperature [see Fig. 5(a)]. A logarithmic temperature dependence in the resistivity might also arise in closely related scenarios as a result of combined disorder and interaction effect (Altshuler-Aronov corrections):[15] (i) the correction to the diffusive transport in two dimensions; (ii) the correction to the tunneling conductivity in two dimensions, and (iii) the correction to the conductivity in systems where the charge diffusion is effectively *zero dimensional*;[47–49] the latter two corrections apply to granular systems.

For *poly*-MTO a precise comparison between theory and experiment is difficult, since we have no information on the granularity or possible current paths through the samples. In the following we discuss in more detail possibility (i) including a crossover from 2D to 3D diffusion. In a simple ansatz we assume that

$$\rho(T) \approx \rho_0 + \alpha\rho_\parallel(T). \tag{3}$$

Here ρ_0 represents a temperature-independent contribution to the resistivity from all mechanisms but the resistivity inside the $\{ReO_2\}_\infty$ layers. $\rho_\parallel$ is the resistivity parallel to the $\{ReO_2\}_\infty$ layers. Due to the two-dimensional character of *poly*-MTO it is reasonable to assume that the resistivity parallel to the planes is much smaller than perpendicular to the planes, $\rho_\perp$. In a macroscopic sample with arbitrary orientations of grains, the contribution to the resistance due to diffusion of the electrons parallel to $\{ReO_2\}_\infty$ layers is then larger than $\rho_\parallel$ but of the same order. This is encoded in the parameter α. α is larger than 1, but still of order of 1 and for simplicity we assume that $\alpha \approx 2$. A quantitative estimation of the resistivity is presented in the following. For the sample shown in Fig. 4(b) the temperature dependence of the resistivity in the temperature range between 2 and 30 K and in zero magnetic field obeys

$$\rho(T) = [3.75 + 2 \times 10^{-2} \ln(T_{min}/T)]\text{m}\Omega\,\text{cm}, \tag{4}$$

with $T_{min}=38$ K. This has to be compared with the theoretical estimate

$$\rho(T) \approx \rho_0 + \frac{\alpha}{e^2 D_\parallel N(E_F) + \delta\sigma_\parallel(T)}, \tag{5}$$

where $D_\parallel$ is the electron diffusion constant parallel to the $\{ReO_2\}_\infty$ layers, and $N(E_F)$ is the density of states at the Fermi energy, given by $N(E_F)=5.2$ states/eV atom$=5.1 \times 10^{28}$ states/eV m^3 (see Sec. III D). An expansion of Eq. (5) for small $\delta\sigma_\parallel(T)$ results in

$$\rho(T) \approx \rho_0 + \alpha\rho_\parallel(T_{min}) - \frac{\alpha}{[e^2 D_\parallel N(E_F)]^2}\delta\sigma_\parallel(T). \tag{6}$$

In two-dimensional systems the Altshuler-Aronov correction[15] (disorder enhanced electron-electron scattering) to the conductivity is

$$\delta\sigma_\parallel(T) = -\frac{e^2}{2\pi^2\hbar}\frac{1}{d}\ln(T_{min}/T), \tag{7}$$

where $d=(7.4\pm0.4)$ Å is the distance between the $\{ReO_2\}_\infty$ layers.[50] Inserting Eq. (7) into Eq. (6) and comparing the theoretical temperature dependence of the resistivity with the experimental finding [Eq. (4)] enables us to estimate $D_\parallel \approx 5 \times 10^{-5}$ m^2/s (with $\alpha=1$ we obtain $D_\parallel \approx 3.5 \times 10^{-5}$ m^2/s) and $\rho_\parallel \approx 0.25$ mΩ cm, i.e., 6% of the total resistance arises due to diffusion in the planes. From the diffusion constant we determine the thermal diffusion length $L_\parallel = \sqrt{\hbar D_\parallel / k_B T} = 87$ Å at 5 K (see Table II) which is clearly smaller than the size of the grains seen in the micrograph in Fig. 1.

Upon lowering the temperature the diffusion becomes three-dimensional with the crossover temperature $k_B T_{co} \approx \hbar D_\perp / d^2$, where $D_\perp$ is the diffusion constant perpendicular to the planes. Experimentally the crossover between a high-temperature $\ln(1/T)$ and a low-temperature $\sqrt{T}$ behavior in the resistivity is observed near 1.5 K, from which we obtain $D_\perp \approx 11 \times 10^{-8}$ m^2/s, and which is considerably smaller than $D_\parallel$ (see Table II). An independent estimate of $D_\perp$ is obtained from the amplitude of the low-temperature square-root dependence of the conductivity $[\delta\sigma_\parallel(T)]$. This theory predicts for a system with anisotropic three-dimensional diffusion

$$\delta\sigma_\parallel(T) = 0.915\frac{e^2}{2\pi^2\hbar}\frac{2}{3}\frac{D_\parallel}{\bar{D}}\left(\frac{k_B T}{\hbar\bar{D}}\right)^{1/2}, \tag{8}$$

with an average diffusion constant $\bar{D} = (D_\parallel^2 D_\perp)^{1/3}$, cf. Refs. 15 and 51. The experimental value is $\delta\rho(T) = 2.2 \times 10^{-7}\ \Omega\,\text{m}\sqrt{T/\text{K}}$, leading to $D_\perp = 2.4 \times 10^{-8}$ m^2/s ($\alpha=1$: $D_\perp = 0.6 \times 10^{-8}$ m^2/s) using Eq. (6). For comparison the estimated values of the diffusion constant $D_\perp$ as deduced in two different ways are listed in Table II: (i) $D_\perp(T_{co})$ from the crossover temperature T_{co} between the $\ln(1/T)$ and $\sqrt{T}$ behavior and (ii) $D_\perp(3D)$ from the coefficient of the $\sqrt{T}$ behavior in Fig. 4(c). Considering the crude nature of Eq. (3), we believe that these results agree surprisingly well.

Poly-MTO intercalated with TTF are treated in the same

TABLE II. In-plane resistivities and diffusion constants for *poly*-MTO and $La_{1.85}Sr_{0.15}Zn_yCu_{1-y}O_4$.

	$x;y$ (%)	$D_\parallel$ (10^{-4} m^2/s)	$\rho_\parallel$ m Ω cm	$D_\perp(T_{co})$ (10^{-8} m^2/s)	$D_\perp$(3D) (10^{-8} m^2/s)	$L_\parallel(T=5$ K) (Å)	T_{co} (K)
poly-MTO		0.50	0.25	11	2.4	87	1.5
poly-MTO+x TTF	2.5	0.50[a]	0.25[a]			87[a]	
	13.5	0.50[a]	0.25[a]			87[a]	
	18.5	0.38	0.32			76	
	30	0.24	0.51	1.5[b]		60	0.2
LSCO+y Zn	0.08	11.9	0.45[c]	23	3.4	426	1
	0.10	10.52	0.61[c]	20	3.5	400	0.9
	0.12	5.9	1.27[c]	4.6	1.0	300	0.2

[a]Within the error bars the gradient of the logarithmic correction is the same as for *poly*-MTO.
[b]For the calculation we used the distance between the $\{ReO_2\}_\infty$ layers of *poly*-MTO as an upper limit.
[c]Here we set $\rho_\parallel$ equal to $\rho_\parallel(T_{min})$ [see Eq. (9)].

way using the data presented in Fig. 5(a). The results are listed in Table II as well. While $\rho_\parallel$ is increasing, $D_\parallel$ is decreasing with increasing TTF amount, attributed to an increasing number of localized electrons at the Re(d^1) sites, which is in line with our scenario. Furthermore, the crossover temperature T_{co} is decreasing with an increasing amount of scattering centers which is reasonable if the distance between the layers increases with increasing TTF concentration ($k_B T_{co} \approx \hbar D_\perp / d^2$).

Finally we comment on the resistivity of $La_{1.85}Sr_{0.15}CuO_4$ doped with Zn, since we believe that the temperature dependence can be explained by the same mechanism as in *poly*-MTO. Experimental data, taken from Ref. 8, are shown in Fig. 16. Already in Ref. 8 it has been noted that the increase in the resistivity is logarithmic in a certain temperature range and it was speculated that the saturation of the resistivity below 300 mK could signal some remanence of the superconducting phase.

Using the microscopic picture from above we start with the ansatz

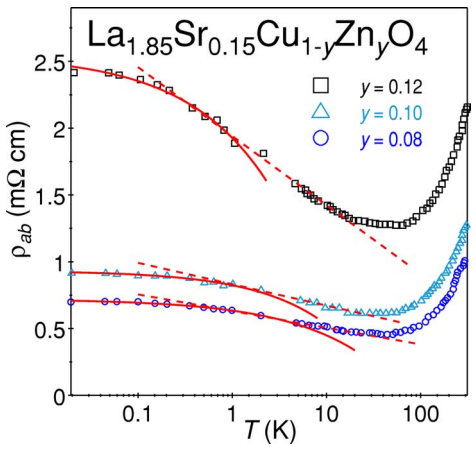

FIG. 16. (Color online) The temperature dependence of the resistivity of $La_{1.85}Sr_{0.15}Cu_{1-y}Zn_yO_4$ with $y=0.08, 0.1, 0.12$. The data are taken from Ref. 8. The lines are fits to the data indicating disorder enhanced electron-electron scattering as discussed in the text [solid lines, $\rho(T) \sim \sqrt{T}$; dashed lines, $\rho(T) \sim \ln(1/T)$] (Ref. 15).

$$\rho_\parallel(T) = \rho_\parallel(T_{min}) - \alpha \rho_\parallel(T_{min})^2 \delta\sigma_\parallel(T), \quad (9)$$

and taking $\delta\sigma$ from Eq. (7) the logarithm is consistently explained with $\alpha=2.85$, 2, and 1.45 for the three Zn concentrations $y=0.08$, 0.1, and 0.12, respectively (here the distance between the $\{CuO_2\}_\infty$ planes is $d=13.2$ Å).[53]

Figure 16 demonstrates that the logarithmic increase of $\rho(T)$ changes—as in *poly*-MTO—to a $\sqrt{T}$ behavior, which we believe is controlled by the crossover from 2D to 3D electron diffusion. Following the same procedure as before we estimate the electron diffusion constants parallel and perpendicular to the $\{CuO_2\}_\infty$ layers. The results are listed in Table II. To obtain the diffusion constant from the conductivity we need the density of states at the Fermi energy which we assume to be given by $N(E_F) \approx 0.36$ states/eV atom $= 9.78 \times 10^{26}$ states/eV m^3, Ref. 52. The ratio $D_\perp / D_\parallel$, which is the ratio of the conductivity perpendicular and parallel to the $\{CuO_2\}_\infty$ planes, is thus estimated to be of the order 10^{-4}, which is a reasonable result for $La_{1.85}Sr_{0.15}Zn_yCu_{1-y}O_4$.

V. CONCLUSION

Summarizing, the inherently conducting organometallic polymer $\{(CH_3)_{0.92}ReO_3\}_\infty$ (*poly*-MTO) is a promising compound for a transition-metal oxide featuring physical properties characteristic for a two-dimensional system. The 2D character of *poly*-MTO is also reflected by the unusual diffraction pattern which can be indexed by a square lattice [$a=3.67(2)$ Å] in conformity with the 2D space group *p4mm*. The pronounced peak shape asymmetry is another characteristic indicator for a layered compound lacking a 3D ordering. We therefore suggest a turbostatic or a 00*l* defect stacking model for the type of disorder, displayed by *poly*-MTO layers along the crystallographic *c* axis. The geometry of the corner sharing CH_3ReO_5 octahedra within the *poly*-MTO layers was optimized by DFT methods resulting in a tungstite-type structural model with alternating Re—CH_3 methyl groups located above and below the $\{ReO_2\}_\infty$ layers, respectively. The presence of methyl groups thus hinders the formation of a 3D oxide network. As a result the layers are nearly ideally decoupled and solely connected

by subtle van der Waals interactions which are reflected particularly by the large 2D phonon contribution in the specific heat. This 2D structure is also confirmed by electrical transport properties. The logarithmic correction to the temperature dependence of the resistivity at high temperature is an important manifestation of a 2D Fermion system.

Below a characteristic temperature T_{min} the resistivity changes from metallic to insulating behavior. This property is intensified by an intercalation of the *poly*-MTO host lattice with donor and acceptor guest molecules leading to a phase diagram which is related to that found for Zn doped high-T_c superconductors such as $La_{1.85}Sr_{0.15}CuO_4$. The origin of metallic behavior of *poly*-MTO is mainly due to a Re($5d$) contribution at the Fermi level as determined by DFT and LDA studies. This preliminary result on the calculated electronic density of states $[N(E_F) \approx 1$ states/eV atom] is roughly of the same order than that obtained from specific heat measurements $[N(E_F) \approx 5.2$ states/eV atom].

The area of the insulating regime is directly related to the amount of localized magnetic moments which was analyzed by means of susceptibility and magnetization measurements. In addition, ESR studies have clearly identified that the main part of these localized electrons is due to the presence of Re(d^1) centers. This result is very important to explain the unexpected positive magnetoresistance in the insulating regime. The susceptibility and ESR measurements on TTF-intercalated *poly*-MTO samples clearly demonstrate that a stronger formation of the positive magnetoresistance is related to an increase of spatially localized electrons. This result is also supported by magnetic field dependent specific heat studies of the nuclear contribution of the ^{185}Re and ^{187}Re quadrupole moments. The electrical field gradient V_{zz} in the vicinity of the Re atoms decreases with increasing external magnetic field indicating a reduction of distortion. This is corroborated by DFT calculations which demonstrate that an enhanced amount of spatially localized electrons leads to a higher symmetry in the vicinity of the Re atoms.

Furthermore, we have now a comprehensive understanding of the logarithmic temperature dependence $\ln(1/T)$ followed by a square-root behavior of the resistivity at low temperatures. Due to spin localization a disorder enhanced electron-electron interaction, as discussed by Altshuler and Aronov, models this behavior very well taking into account a crossover from a 2D to a 3D system at very low temperatures. Due to the large chemical variation possibilities, *poly*-MTO and its intercalated species represent promising candidates to stimulate the field of functional two-dimensional systems.

ACKNOWLEDGMENTS

This work was supported by the Deutsche Forschungsgemeinschaft (DFG) through the SFB 484, the SPP 1178, by the COST P16-ECOM project of the European Union, and by NanoCat, an international graduate program within the Elitenetzwerk Bayern.

*Electronic address: Wolfgang.Scherer@Physik.Uni-Augsburg.de

[1] W. A. Herrmann, R. W. Fischer, and W. Scherer, Adv. Mater. (Weinheim, Ger.) **4**, 653 (1992).

[2] W. A. Herrmann, W. Scherer, R. W. Fischer, J. Blümel, M. Kleine, W. Mertin, R. Gruehn, J. Mink, H. Boysen, C. C. Wilson, R. M. Ibberson, L. Bachmann, and M. Mattner, J. Am. Chem. Soc. **117**, 3231 (1995).

[3] R. W. Fischer, Ph.D. thesis, TU München, 1994.

[4] H. S. Genin, K. A. Lawler, R. Hoffmann, W. A. Herrmann, R. W. Fischer, and W. Scherer, J. Am. Chem. Soc. **117**, 3244 (1995).

[5] R. Miller, C. Helbig, G. Eickerling, R. Herrmann, E. W. Scheidt, and W. Scherer, Physica B **359–361**, 448 (2005).

[6] E.-W. Scheidt, R. Miller, C. Helbig, G. Eickerling, F. Mayr, R. Herrmann, P. Schwab, and W. Scherer, cond-mat/0504585 [Physica B (to be published)].

[7] K. Segawa and Y. Ando, Phys. Rev. B **59**, R3948 (1999).

[8] K. Karpińska, M. Z. Cieplak, S. Guha, A. Malinowski, T. Skośkiewicz, W. Plesiewicz, M. Berkowski, B. Boyce, T. R. Lemberger, and P. Lindenfeld, Phys. Rev. Lett. **84**, 155 (2000).

[9] Y. Ando, G. S. Boebinger, A. Passner, T. Kimura, and K. Kishio, Phys. Rev. Lett. **75**, 4662 (1995).

[10] G. S. Boebinger, Y. Ando, A. Passner, T. Kimura, M. Okuya, J. Shimoyama, K. Kishio, K. Tamasaku, N. Ichikawa, and S. Uchida, Phys. Rev. Lett. **77**, 5417 (1996).

[11] J. Bobroff, W. A. MacFarlane, H. Alloul, P. Mendels, N. Blanchard, G. Collin, and J.-F. Marucco, Phys. Rev. Lett. **83**, 4381 (1999).

[12] F. Rullier-Albenque, H. Alloul, and R. Tourbot, Phys. Rev. Lett. **87**, 157001 (2001).

[13] X. G. Luo, X. H. Chen, X. Liu, R. T. Wang, C. H. Wang, L. Huang, L. Wang, and Y. M. Xiong, Supercond. Sci. Technol. **18**, 234 (2005).

[14] C. M. Varma, Phys. Rev. Lett. **79**, 1535 (1997).

[15] B. L. Altshuler and A. G. Aronov, in *Electron-Electron Interaction in Disordered Systems*, edited by A. L. Efros and M. Pollak, (North-Holland Amsterdam, 1985).

[16] S. Y. Li, W. Q. Mo, X. H. Chen, Y. M. Xiong, C. H. Wang, X. G. Luo, and Z. Sun, Phys. Rev. B **65**, 224515 (2002).

[17] W. A. Herrmann and R. M. Kratzer, Inorg. Synth. **33**, 110 (2002).

[18] W. A. Herrmann and R. W. Fischer, J. Am. Chem. Soc. **117**, 3223 (1995).

[19] K. Z. Meisel, Z. Anorg. Allg. Chem. **207**, 121 (1932); P. Kiprof, W. A. Hermann, F. E. Kühn, W. Scherer, M. Klein, M. Elison, K. Rypdal, H. V. Volden, S. Gundersen, and A. Haaland, Bull. Soc. Chim. Fr. **129**, 655 (1992).

[20] C. Helbig, R. Herrmann, F. Mayr, E.-W. Scheidt, K. Tröster, J. Hanss, H.-A. Krug von Nidda, G. Heymann, H. Huppertz, and W. Scherer, Chem. Commun. (Cambridge) **2005**, 4071.

[21] For patterns i-iv a Bragg-Brentano device with Cu K_α radiation, for pattern v a Guinier camera with Mo K_α radiation has been used.

[22] M. J. Frisch, G. W. Trucks, H. B. Schlegel, G. E. Scuseria, M. A. Robb, J. R. Cheeseman, J. A. Montgomery, Jr., T. Vreven, K. N. Kudin, J. C. Burant, J. M. Millam, S. S. Iyengar, J. Tomasi, V.

Barone, B. Mennucci, M. Cossi, G. Scalmani, N. Rega, G. A. Petersson, H. Nakatsuji, M. Hada, M. Ehara, K. Toyota, R. Fukuda, J. Hasegawa, M. Ishida, T. Nakajima, Y. Honda, O. Kitao, H. Nakai, M. Klene, X. Li, J. E. Knox, H. P. Hratchian, J. B. Cross, V. Bakken, C. Adamo, J. Jaramillo, R. Gomperts, R. E. Stratmann, O. Yazyev, A. J. Austin, R. Cammi, C. Pomelli, J. W. Ochterski, P. Y. Ayala, K. Morokuma, G. A. Voth, P. Salvador, J. J. Dannenberg, V. G. Zakrzewski, S. Dapprich, A. D. Daniels, M. C. Strain, O. Farkas, D. K. Malick, A. D. Rabuck, K. Raghavachari, J. B. Foresman, J. V. Ortiz, Q. Cui, A. G. Baboul, S. Clifford, J. Cioslowski, B. B. Stefanov, G. Liu, A. Liashenko, P. Piskorz, I. Komaromi, R. L. Martin, D. J. Fox, T. Keith, M. A. Al-Laham, C. Y. Peng, A. Nanayakkara, M. Challacombe, P. M. W. Gill, B. Johnson, W. Chen, M. W. Wong, C. Gonzalez, and J. A. Pople, GAUSSIAN03 (Gaussian, Inc., Wallingford, CT, 2004).

[23] J. S. Binkley, J. A. Pople, and W. J. Hehre, J. Am. Chem. Soc. **102**, 939 (1980); R. B. Ross, J. M. Powers, T. Atashroo, W. C. Ermler, L. A. LaJohn, and P. A. Christiansen, J. Chem. Phys. **93**, 6654 (1990).

[24] J. P. Perdew, K. Burke, and M. Ernzerhof, Phys. Rev. Lett. **77**, 3865 (1996); **78**, 1396 (1997).

[25] J. T. Szymanski and A. C. Roberts, Can. Mineral. **22**, 681 (1984).

[26] J. Mink, G. Keresztury, A. Stirling, and W. A. Herrmann, Spectrochim. Acta, Part A **50A**, 2039 (1994).

[27] In a previous publication (Ref. 6) the high temperature resistivity data were fitted with a $T^{3/2}$ dependence. Since no convincing model for this T behavior exists, we present an alternative approach in this paper.

[28] M. Kaveh and N. Wiser, Adv. Phys. **33**, 257 (1984).

[29] C. C. Tsuei, A. Gupta, and G. Koren, Physica C **161C**, 415 (1989).

[30] G. F. Giuliani and J. J. Quinn, Phys. Rev. B **26**, 4421 (1982).

[31] L. Zheng and S. DasSarma, Phys. Rev. B **53**, 9964 (1996).

[32] S. Martin, M. Gurvitch, C. E. Rice, A. F. Hebard, P. L. Gammel, R. M. Fleming, and A. T. Fiory, Phys. Rev. B **39**, R9611 (1989).

[33] Note the surprising result that acceptor ligands intercalate a rather electron deficient oxide host lattice at all!

[34] P. Fournier, P. Mohanty, E. Maiser, S. Darzens, T. Venkatesan, C. J. Lobb, G. Czjzek, R. A. Webb, and R. L. Greene, Phys. Rev. Lett. **81**, 4720 (1998).

[35] S. Ono, Y. Ando, T. Murayama, F. F. Balakirev, J. B. Betts, and G. S. Boebinger, Phys. Rev. Lett. **85**, 638 (2000).

[36] The molar core diamagnetism is roughly estimated using $\chi_{\mathrm{dia}}^{\mathrm{Langevin}} = -0.79 Z_i \times 10^{-6} \langle (r/a_0)^2 \rangle$ emu/mol, where Z_i is the sum of all core electrons per formular unit (for pure *poly*-MTO $Z_i = 88$) and $\langle (r/a_0)^2 \rangle = 1$ with a_0 the Bohr radius. Therefore, χ_0 and the resulting χ_{P} are furnished with an error bar of 30%.

[37] S. E. Barnes, Adv. Phys. **30**, 801 (1981).

[38] A. Voigt, U. Abram, R. Böttcher, U. Richter, J. Reinhold, and R. Kirmse, Chem. Phys. **253**, 171 (2000).

[39] J. F. Gibson, G. M. Lack, K. Mertis, and G. Wilkinson, J. Chem. Soc. Dalton Trans. **1976**, 1492.

[40] R. Bachmann, F. J. DiSalvo, T. H. Geballe, R. L. Greene, R. E. Howard, C. N. King, H. C. Kirsch, K. N. Lee, R. E. Schwall, H. U. Thomas, and R. B. Zubeck, Rev. Sci. Instrum. **43**, 205 (1972).

[41] L. J. Morris, A. J. Downs, T. M. Greene, G. S. McGrady, W. A. Herrmann, P. Sirsch, W. Scherer, and O. Gropen, Organometallics **20**, 2344 (2001).

[42] A. R. Williams, J. Kübler, and C. D. Gelatt, Jr., Phys. Rev. B **19**, 6094 (1979).

[43] V. Eyert, Int. J. Quantum Chem. **77**, 1007 (2000).

[44] More accurate calculations using a fine **k**-point mesh for the Brillouin zone integration as well as the generalized gradient approximation instead of the LDA are in progress.

[45] W. Scherer, R. Herrmann, K. Tröster, S. Altmannshofer, G. Eickerling, C. Helbig, and F. Mayr (unpublished); G. Eickerling, Ph.D. thesis, Augsburg, 2006.

[46] D. L. Cox and A. Zawadowski, Adv. Phys. **47**, 599 (1998).

[47] P. Schwab and R. Raimondi, Eur. Phys. J. B **30**, 5 (2002).

[48] P. Schwab and R. Raimondi, Ann. Phys. **12**, 471 (2003).

[49] I. S. Beloborodov, A. V. Lopatin, and V. M. Vinokur, Phys. Rev. B **70**, 205120 (2004).

[50] The interlayer distance of 7.4 Å can be derived from the structure of intercalated *poly*-MTO ($H_{0.5}[(CH_3)_{0.92}ReO_3]$), which was determined by *x*-ray diffraction techniques. This compound displays double layers of *poly*-MTO with an interlayer distance of 7.4 Å, which are separated from each other by a layer of water molecules (see Ref. 2 for further details).

[51] R. N. Bhatt, P. Wölfle, and T. V. Ramakrishnan, Phys. Rev. B **32**, 569 (1985).

[52] M. Schossmann, F. Marsiglio, and J. P. Carbotte, Phys. Rev. B **36**, 3627 (1987).

[53] P. Day, M. Rosseinsky, K. Prassides, W. I. F. David, O. Moze, and A. Soper, Solid State Phys. **20**, L429 (1987).